Simulation of Cloud Microphysical and Chemical Processes Using a Multicomponent Framework. Part I: Description of the Microphysical Model

JEN-PING CHEN* AND DENNIS LAMB

Department of Meteorology, The Pennsylvania State University, University Park, Pennsylvania

(Manuscript received 2 July 1993, in final form 22 February 1994)

ABSTRACT

A detailed microphysical and chemical cloud model has been developed to investigate the redistribution of atmospheric trace substances through cloud processes. A multicomponent categorization scheme is used to group cloud particles into different bins according to their various properties. Cloud drops are categorized simultaneously and independently in both their water mass and solute mass components. Ice phase particles are additionally categorized according to their "shapes," special effort having been paid to the parameterization of their growth and habit changes. The hybrid bin method used conserves the mass and number of particles while at the same time performing fast and accurate calculations for transferring various properties between categories within the multicomponent framework. With a minimum of parameterization, this model is capable of simulating detailed microphysical and chemical processes that occur during cloud and precipitation formation.

1. Introduction

Cloud is the dominant place in the atmosphere where trace constituents can exist in a condensed phase. These constituents become partially or wholly dissolved in the cloud water, sorbed by cloud ice, or fixed in a nonvolatile form by means of chemical transformations that may not be significant elsewhere in the atmosphere. Constituents that are particularly soluble or nonvolatile tend to be removed effectively from the atmosphere by precipitation processes and deposited onto the earth's surface. Thus, cloud processes have the general effect of cleansing the atmosphere and offsetting some air pollution problems, although at the expense of creating other problems such as wet acidic deposition. Those trace chemicals not deposited by a particular storm system become redistributed within the upper troposphere and enter the global background atmosphere. There, they may affect the global radiation budget and further influence the chemistry of the atmosphere. Particulate forms of the trace chemicals, modified in both composition and number concentration, can again serve as cloud-forming nuclei for later cloud development and thus alter precipitation and deposition patterns in nonlinear ways. The trace chemicals can also interact with the biosphere and cause nonlinear feedback effects on the climate (Charlson et al. 1987). Such effects, whether short term or long term, are interrelated through cloud processes. Any disturbance to one component will affect the others. Therefore, it is all the more important that we learn to understand the physical and chemical processes involved in clouds.

Numerical simulation is currently an active means for studying the physics and chemistry of clouds. Due to limitations of computer resources and imperfect knowledge of the subject, each numerical modeling effort must focus on some aspect of the problem and use simplifications and parameterizations to some degree. For instance, Tripoli and Cotton (1982), as well as Lin et al. (1983), used bulk water parameterizations to describe the microphysics in two-dimensional dynamic models. Sarma (1986) similarly incorporated sulfate chemistry into a bulk water model. Clark (1973) included detailed liquid phase microphysics in a two-dimensional model to study warm cumulus convection. Hall (1980) used a two-dimensional slab-symmetric dynamic framework and a detailed treatment of both liquid and ice phase particles. Flossmann and Pruppacher (1988) extended Hall's work with the addition of aerosol scavenging and equilibrium chemistry for some sulfur compounds, but they neglected cold-cloud (ice phase) processes. Tremblay and Leighton (1986), as well as Niewiadomski (1989), used a three-dimensional model with parameterized warm rain development and kinetic oxidation of sulfur dioxide to simulate the convective and turbulent transport of sulfur species. Pandis and Seinfeld (1989), as well as Topalian and Montague (1989), used a very detailed kinetic reaction

* Also affiliated with the Center for Clouds, Chemistry and Climate, Scripps Institution of Oceanography.

Corresponding author address: Dr. Jen-Ping Chen, Dept. of Atmospheric Sciences, National Taiwan University, Taipei, Taiwan, Republic of China.

scheme of the aqueous phase chemistry for the scavenging of pollutant gases, but included no microphysics or dynamics. Giorgi and Chameides (1985) used a first-order parameterization to simulate rainout in a photochemical model within a general circulation model without explicit cloud physics.

The evolution of cloud chemistry research has demonstrated the necessity of using more detailed physics and chemistry. Studies of Hegg and Hobbs (1988), as well as Lamb and Chen (1988), showed that microphysical processes in clouds can have significant influence on the fractionation and the removal efficiency of chemicals in clouds. Cho et al. (1989), Lamb and Chen (1990), and Chen and Lamb (1990) have demonstrated that ice phase microphysics can play an important role in the scavenging of trace chemicals by clouds. Therefore, a detailed model with adequate microphysics in both liquid and ice phases is necessary for a proper calculation of the chemistry in clouds.

The purpose of this study is to develop a numerical scheme for simulating the microphysical and chemical processes of clouds, with particular emphasis being placed on the ice phase. A multicomponent particle framework is applied that categorizes (bins) cloud particles not only according to their mass (or size) but also according to their solute content and, for ice particles, their shapes. Some preliminary results using such a multicomponent particle framework have been presented by Chen and Lamb (1992) for liquid-phase processes and by Chen and Lamb (1994) for the depositional growth of ice particles. A similar study applying such a multicomponent structure has been done by Roelofs (1992), but for liquid-phase processes only. Here, we treat both liquid and ice phase processes in detail using the multicomponent framework. This paper describes the mixed-phase microphysics and chemistry needed for this study, as well as the numerical methods used. The results of the model simulation on the redistribution of atmospheric trace substances through cloud processes will be presented in subsequent papers.

2. The numerical model and methods of solution

a. Multicomponent particle framework

The evolution of atmospheric particles in size or composition usually cannot be solved analytically. Conventional cloud models often group cloud particles into relatively few categories and are normally called bulk water models (e.g., Kessler 1969; Clark 1974; Tripoli and Cotton 1982; Lin et al. 1983; Mitchell 1991; Wang and Chang 1993). However, these bulk water methods often are not sufficient to describe the true particle spectra, especially for the ice-phase particles. Moreover, individual cloud particles act differently from bulk water in nonlinear ways. Bulk water parameterizations may therefore give misleading results in cloud chemistry (Hegg 1989; Hegg and Larson 1990).

By contrast, detailed cloud models allow the cloud particle spectra to evolve naturally according to explicit physics (e.g., Flossmann et al. 1985; Tzivion et al. 1987; Ayers and Larson 1990) by categorizing particles into many more size bins. One or more parameters (moments) are then used to describe the distribution of particles in each bin. These detailed models are often called bin models or category models. Most bin models, however, resolve the particle spectra according to the particle size or mass only. In such models, all particles of the same size necessarily have exactly the same physical and chemical properties. Theoretical studies of Hill (1988), Hegg and Larson (1990), and Chen and Lamb (1992), as well as the experimental study of Noone et al. (1988) and Ogren et al. (1989), showed that it is important to consider the drop size–dependent solute concentration. The condensation model of Johnson (1982) applied five "solubility" categories to each of the mass bins. Yet, since interactions between particles in different bins were not allowed, that model could not be used to study collisional processes.

The properties of ice particles are especially complicated because ice particles that have the same mass do not necessarily have the same size or shape. Conventional detailed cloud models are not able to resolve the complicated shapes of ice particles and their growth habits, which are important factors that control both the ice-phase microphysics and chemistry. Those models that have considered the shapes of ice crystals tended to overlook the possible changes of primary habits or the temperature and supersaturation dependence of the secondary habits (Hindman and Johnson 1972; Hall and Pruppacher 1976; Miller and Young 1979). None of these models was able to describe the change with time of the shapes of ice crystals due to vapor deposition, riming, or aggregation under varying ambient conditions.

The multicomponent framework described here categorizes cloud particles simultaneously and independently according to their various physical and chemical properties. In order to describe the liquid cloud particles, a mass component m_s for one major solute (usually sulfate) is used in addition to the usual water mass component m_w. The representation of ice-phase particles requires a separate framework. One physical parameter that distinguishes the ice-phase particles from the liquid-phase particles is their shapes. Thus, a shape factor ϕ (axial ratio of a representative spheroid) is included in the ice particle framework in addition to the properties used in the liquid-phase particle framework. In this study, 45, 20, and 11 bins are used for the water mass, solute mass, and shape components, respectively. Note that other minor physical and chemical properties of the particles (e.g., temperature, density, minor solute masses) do not require detailed bin resolution.

The equation for the evolution of the number density of liquid-phase particles n_d is written as (cf. Clark 1973; Hall 1980; Flossmann et al. 1985)

$$\frac{\partial n_d}{\partial t} = -\nabla\cdot(\mathbf{V}n_d) + \frac{\partial}{\partial z}(V_\infty n_d) + C, \qquad (1)$$

where $\mathbf{V}$ is the air velocity and V_∞ is the terminal fall speed of the drop. The first two terms on the right-hand side represent the effects of advection and sedimentation, respectively. The last term represents changes of n_d due to microphysical and chemical processes, the main focus of this paper. Aside from any spatial dependence, n_d is a function of (m_w, m_s, t) and has units of (kg water)$^{-1}$ (kg solute)$^{-1}$ (kg air)$^{-1}$. The changes of n_d can then be subdivided into the changes in the components m_w and m_s:

$$C = \left.\frac{\partial n_d}{\partial t}\right|_{\text{adv},w} + \left.\frac{\partial n_d}{\partial t}\right|_{\text{adv},s} + C_w + C_s, \qquad (2)$$

where the subscripts "w" and "s" denote the water and solute components, respectively. The first two terms on the right-hand side represent processes that do not involve other particles, such as water vapor condensation (m_w component) or trace gas sorption and chemical production of solute (m_s component). They are commonly expressed in a form similar to the advection term in (1) (cf. Clark 1973; Hall 1980; Flossmann et al. 1985):

$$\left.\frac{\partial n_d}{\partial t}\right|_{\text{adv},w} = -\frac{\partial}{\partial m_w}\left(n_d\frac{dm_w}{dt}\right) \qquad (3a)$$

$$\left.\frac{\partial n}{\partial t}\right|_{\text{adv},s} = -\frac{\partial}{\partial m_s}\left(n_d\frac{dm_s}{dt}\right), \qquad (3b)$$

except that the advection is along the component axes (m_w and m_s) instead of along the spatial coordinates. In spectral space, the growth rates dm_w/dt and dm_s/dt serve as analogs to the advection velocities that appear in physical space. The last two terms in (2) represent processes involving other particles, such as coalescence and breakup. For example, C_w and C_s for the coalescence process are represented by the stochastic collection equations (cf. Telford 1955):

$$C_w = \left.\frac{\partial n_d(v_w)}{\partial t}\right|_{\text{coal}} = -n_d(v_w)\int_0^\infty K(v_w, u_w)n_d(u_w)du_w + \frac{1}{2}\int_0^{v_w} K(v_w - u_w, u_w) \times n_d(v_w - u_w)n_d(v_w)du_w \qquad (4a)$$

$$C_s = \left.\frac{\partial n_d(v_s)}{\partial t}\right|_{\text{coal}} = -n_d(v_s)\int_0^\infty K(v_w, u_w)n_d(u_s)du_s + \frac{1}{2}\int_0^{v_s} K(v_w - u_w, u_w) \times n_d(v_s - u_s)n_d(v_s)du_s, \qquad (4b)$$

where u and v are the masses (in either m_w or m_s component) of the colliding particles and K is the particle interaction kernel. Note that the interaction kernels in (4b) are expressed as a function of the water masses because the solute masses normally contribute little to the drop sizes. The change of the number density function $n_i(m_w, m_s, \phi, t)$ of ice-phase particles due to microphysical and chemical factors can similarly be written as

$$C' = \left.\frac{\partial n_i}{\partial t}\right|_{\text{adv},w} + \left.\frac{\partial n_i}{\partial t}\right|_{\text{adv},s} + \left.\frac{\partial n_i}{\partial t}\right|_{\text{adv},\phi} + C'_w + C'_s + C'_\phi, \qquad (5)$$

where the subscript ϕ denotes the shape factor component and n_i has units of (kg water)$^{-1}$ (kg solute)$^{-1}$ (unit ϕ)$^{-1}$ (kg air)$^{-1}$. The moment-conserving scheme discussed next is used to solve the above time evolution of particle spectra within the multicomponent framework.

b. The hybrid bin method

Bin models group particles of similar properties into representative "bins" to reduce the particle population to a manageable number of systems. The *total particle number* in each bin category is introduced as the grouping parameter. Due to growth or decay or to trace–chemical interactions, particles will transfer between bins in the framework. Various numerical methods have been developed to solve the particle transfer problem. For example, Berry (1967), Berry and Reinhardt (1974), Gelbard and Seinfeld (1978), and Flossmann et al. (1985) used a semi-Lagrangian scheme that calculates the growth of particles at discrete grid points. The new values are then interpolated back to the original grid points. However, their method does not guarantee the conservation of mass and is rather time consuming (Tzivion et al. 1987). Young (1974a) circumvented this problem by developing a bin method that assumes a linear distribution function within a bin. Knowledge of the total number and the aggregate bin property value (e.g., total particle mass) allows the linear distribution function to be determined from conservation laws. Young's continuous-bin method is conceptually similar to the method of moments proposed by Stieltjes (1894) and Golovin (1963), which has been applied by Drake (1972), Enukashvilly (1980),

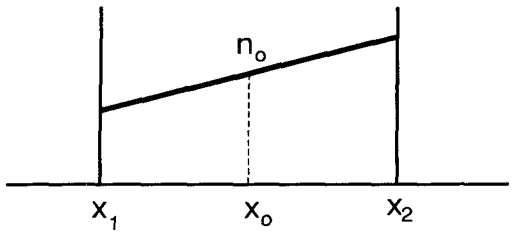

FIG. 1. Linear distribution function of two moments.

Tzivion (1980), and Tzivion et al. (1987). These moment-conserving schemes are highly accurate but less flexible in dealing with different growth kernels and bin-sizing factors.

In this study, we have used a *hybrid bin method,* an approach that is very flexible and conceptually easy to understand. The hybrid bin method calculates the total growth of particles in each bin using their mean masses. By conserving two moments (number and mass), the continuous bin method, which is similar to Young's method, is then used for the transfer of particles between bins. The following gives the details of the hybrid bin method.

1) SUBGRID LINEAR DISTRIBUTION FUNCTION

The distribution of a number density function within a given grid interval (bin) can be approximated by a linear equation with knowledge of the first two moments. The number density function, as shown in Fig. 1, is assumed to be linearly continuous within a bin and is expressed as

$$n(x) = n_0 + k(x - x_0), \tag{6}$$

where x is the independent variable of the number density function, n_0 is the number density at the midpoint x_0 of the bin, and k is the slope of the distribution function. Examples of the independent variable x are m_w, m_s, and ϕ, as discussed previously. The hybrid bin method does not operate on the number density function itself; rather, it keeps track of the two moments. From the law of conservation, the total number N (zeroth moment) and the total or aggregate bin property M (first moment) can be expressed as

$$N = \int_{x_1}^{x_2} n(x)dx, \quad M = \int_{x_1}^{x_2} xn(x)dx, \tag{7}$$

where x_1 and x_2 are, respectively, the lower and upper limits of the bin. Take the most frequently considered property—mass—as an example; then x is the particle mass and M is the total mass of particles in the bin. By inserting (6) into (7), n_0 and k can be derived as

$$n_0 = \frac{N}{x_2 - x_1}, \quad \text{and} \quad k = \frac{12(M - x_0N)}{(x_2 - x_1)^3}, \tag{8}$$

where $x_0 = (x_1 + x_2)/2$. Note that N is the number of particles per kilogram of air and M has the units of x per kilogram of air. The number density function can readily be derived from the knowledge of N and M for calculations that involve particle spectra. By way of example, Fig. 2 demonstrates how the linear distribution function approximates a sinusoidal curve with a rather high accuracy. Since the linear distribution function is only a first-order approximation, the physically unrealistic discontinuities at the bin boundaries (e.g., at $x = 7$ in Fig. 2) are inevitable. Whereas it is possible to use a higher-order form of (6) that would eliminate discontinuities at the bin boundaries (Chen 1992, p. 111), such elaboration is not necessary. As will be shown in the examples given in section 5, such discontinuities do not cause serious numerical problems.

The number density functions representing the cloud particles tend to be discontinuous in nature. As a result, the linear number density function given in (6) may occasionally become negative (see Fig. 3a), especially for bins containing the boundaries of the actual spectrum. Violation of the positiveness condition will lead to unrealistic negative numbers of particles, as well as numerical diffusion. Enukashvilly (1980) treated the problem by applying a zeroth-order approximation function, which forces the distribution function to be zero at the initially negative end, as shown in Fig. 3b, to ensure the positiveness. To be more realistic, however, the distribution function should be allowed to occupy only part of the bin, as demonstrated in Fig. 3c. Thus, once either $n(x_1)$ or $n(x_2)$ is found to be less than zero with the k and n_0 derived previously, the distribution function should be modified as

$$n(x) = k_*(x - x_*). \tag{9}$$

The parameters x_* and k_* are derived by inserting this modified distribution function back into (7) such that

$$x_* = \frac{3M}{N} - 2x_2, \; k_* = \frac{2N}{(x_2 - x_0)^2}, \text{ for } n(x_1) < 0,$$

$$x_* = \frac{3M}{N} - 2x_1, \; k_* = \frac{-2N}{(x_1 - x_0)^2}, \text{ for } n(x_2) < 0. \tag{10}$$

The piecewise linear distribution function (6) can be applied directly into growth equations (1) through (5). However, the problem of closure occurs when the growth kernel is a high-order polynomial. Moreover, the growth equation is often impossible to solve when the growth kernel is transcendental. To avoid such problems, we separate the growth calculation from the particle transfer scheme. This separation is done by first applying the *semidiscrete bin method,* which assumes that all particles in the bin have the same average properties, to calculate the total growth. In other words, we use the "growth of the mean" $d\bar{x}/dt$ to represent the

"mean growth" ($\overline{dx/dt}$). The condensation process, for example, can be represented by

$$\frac{dx}{dt} = Bsx^{1/3}, \tag{11}$$

where x represents the mass of the drop, B is a constant, and s is the supersaturation. Then, the overall mass growth [e.g., Eq. (3a) integrated from x_1 to x_2] for drops in a bin during time interval δt is approximately

$$\delta M = NB\bar{s}\bar{x}^{1/3}\delta t, \tag{12}$$

where $\bar{x} = M/N$ and $\bar{s}$ is the mean saturation ratio during time δt. Similarly, the overall mass growth for drops in bin i by collecting drops in bin j due to coalescence is approximated as

$$\delta M = N_i N_j \bar{x}_j K(\bar{x}_i, \bar{x}_j)\delta t, \tag{13}$$

where $K(\bar{x}_i, \bar{x}_j)$ is the collection kernel between drops of masses $\bar{x}_i$ and $\bar{x}_j$. The new total mass (before performing the bin shift) is then $M' = M + \delta M$, while the total number N remains unchanged. The transfer of particles between bins will then be performed using the bin-shift method described in the next subsection. The hybrid bin method yields results that are quite accurate for small enough bin sizes, and if necessary, a modification factor is available to account for any nonlinearities (Chen 1992, p. 120). This hybrid scheme can vastly reduce the complexity of the governing equations and the computational time.

2) BIN SHIFT

Bin shift is conceptually very similar to advection in Eulerian coordinates. If the component variable x is the distance, the growth rate dx/dt would then be the advection velocity. The bin shift is accomplished by first calculating the growth (advection) in a Lagrangian coordinate and then remapping the new distribution back into the original coordinate. Normally, one would derive the linear distribution function (6) that occurs "before" the growth, as done by Young (1974a). However, an advantage of separating the growth scheme from the bin-shift scheme is that we can alternatively assume that the distribution function is linear "after" the growth. We will call the former *the pregrowth linear method* and the latter *the postgrowth linear method.*

In the pregrowth linear method, a linear distribution function is derived using the total number and mass before the growth, and the distribution function is assumed to maintain its linearity (slope) during the growth (i.e., use N and M to obtain n_0, x_0, and k). As illustrated in Fig. 4a, each of the bin limits would be shifted the same as the change in the midpoint (x_0). In order to maintain the original slope of the distribution, clearly, one must assume that every particle in the bin grows at the same rate. Such an assumption is appropriate only when the growth rate dx/dt is independent of x.

When the growth equations are nonlinear with respect to x, the shift of the two bin limits and the mean may not be exactly the same, resulting in a change of slope. The originally linear distribution function then becomes nonlinear after growth, and a straightforward linear bin shift would not always yield an accurate calculation. This problem can be avoided by applying the *postgrowth linear method.* The new total mass, $M' = M + \delta M$, of the postgrowth distribution is derived as before from the decoupled semidiscrete scheme. In contrast to the pregrowth linear method, however, we now have the freedom of calculating the two new bin limits independently, as shown in Fig. 4b. For a known growth function dx/dt, the shifts of the bin limits δx_1 and δx_2 are calculated in the same way that $\delta\bar{x}$ is. In the case of condensational growth, when (11) is applicable, the approximations $\delta x_1 \approx \delta\bar{x}(x_1/\bar{x})^{1/3}$ and $\delta x_2 \approx \delta\bar{x}(x_2/\bar{x})^{1/3}$ can be used to avoid the generally more complicated growth calculation. For the coalescence growth of drops in bin i collecting drops in bin j, the shifts of the bin limits are simply $\delta x_1 = x_{j,1}$ and $\delta x_2 = x_{j,2}$, where $x_{j,1}$ and $x_{j,2}$ are the bin limits of bin j. Note that the component variable x_i and x_j here can be either the water mass or solute mass for collectional growth processes (e.g., coalescence, riming). The n_0 and k of the new distribution function can be derived by applying the total number N, new total mass $M' = M + \delta M$, and the two new bin limits $x_1' = x_1 + \delta x_1$ and $2x_2' = x_2 + \delta x_2$ to (8). The postgrowth linear method has the advantage over the pregrowth linear method by accounting for the slope change of the distribution function, but it has the disadvantage of requiring calculations of δx_1 and δx_2. If the growth rates at the bin limits x_1 and x_2 are unknown or do not have a clear relationship to the shift of $\bar{x}$, as discussed in the above examples, then the pregrowth linear method must be used. Otherwise, the postgrowth linear method provides better accuracy and is preferred.

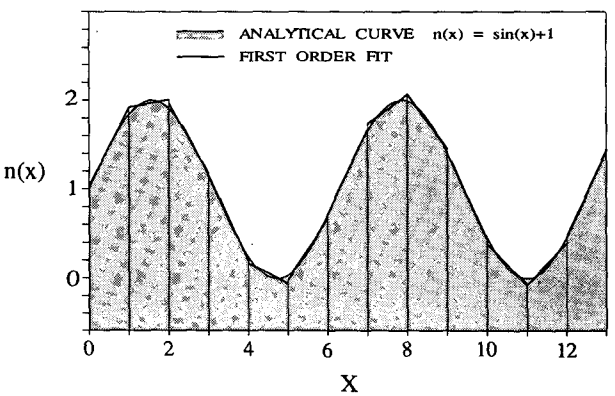

FIG. 2. First-order approximation of the curve $n(x) = \sin(x) + 1$ using the continuous-bin method.

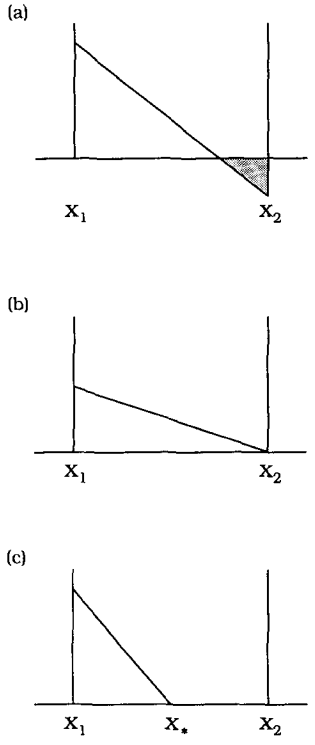

FIG. 3. Positiveness of the linear distribution function: (a) before adjustment, (b) Enukashvilly's zeroth-order approximation, and (c) method proposed here.

The particles in that part of the distribution that exceed the original bin limits during growth must be transferred to the next bin. The number and mass that need to be transferred can be determined by the following functions:

$$\Delta N = f_N(n_0, x_0, k, x_2, x_2');$$
$$\Delta M = f_M(n_0, x_0, k, x_2, x_2') \quad \text{for} \quad \delta x > 0,$$
$$\Delta N = f_N(n_0, x_0, k, x_1', x_1);$$
$$\Delta M = f_M(n_0, x_0, k, x_1', x_1) \quad \text{for} \quad \delta x < 0, \quad (14)$$

where δx $(=\delta M/N)$ is the mean growth over the time step δt, and f_N and f_M are defined as

$$f_N(n_0, x_0, k, a, b) \equiv \int_a^b n(x)dx = (b-a)\left[n_0 - k\left(x_0 - \frac{a+b}{2}\right)\right],$$

$$f_M(n_0, x_0, k, a, b) \equiv \int_a^b xn(x)dx = n_0\frac{b^2-a^2}{2} + k\left(\frac{b^3-a^3}{3} - x_0\frac{b^2-a^2}{2}\right), \quad (15)$$

where a and b are the appropriate lower and upper integration limits, respectively. The total number and mass left in the original bin are thus

$$N' = N - \Delta N,$$
$$M' = (M + \delta M) - \Delta M, \quad (16)$$

where δM is from the semidiscrete method mentioned previously. The same principle applies when the distribution shifts over multiple grids.

The positiveness check mentioned previously is important for reducing numerical diffusion and ensuring the conservation law. With the positiveness check, particle transfer is not always performed in each time step. The new distribution may still lie within the range of the original bin limits, as shown in Fig. 4c. When the positiveness criterion is violated, the number and mass that need to be transferred can still be determined from (14) by applying new parameters x_* and k_* so that when $\delta x > 0$,

$$\Delta N = 0; \quad \Delta M = 0, \quad \text{for} \quad x_* < x_2$$
$$\Delta N = f_N(0, x_*, k_*, x_2, x_2');$$
$$\Delta M = f_M(0, x_*, k_*, x_2, x_2') \quad \text{for} \quad n(x_1) < 0$$
$$\Delta N = f_N(0, x_*, k_*, x_2, x_*);$$
$$\Delta M = f_M(0, x_*, k_*, x_2, x_*) \quad \text{for} \quad n(x_2) < 0 \quad (17a)$$

and when $\delta x < 0$,

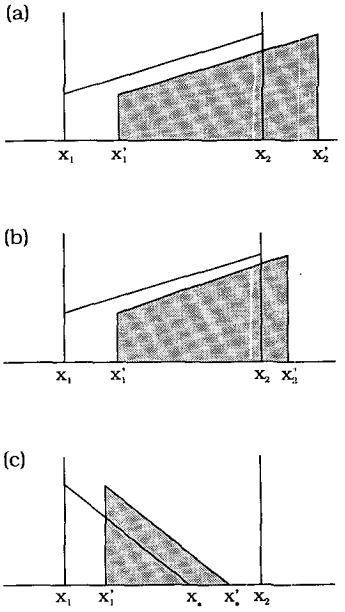

FIG. 4. Schematic diagram of (a) the pregrowth linear distribution function and the bin shift (the two bin limits shifted by the same amount), (b) the postgrowth linear method (the two bin limits shift by different amounts), and (c) incomplete distribution, where the white area is the original distribution and the shaded area denotes the new distribution.

$$\Delta N = 0, \quad \Delta M = 0, \quad \text{for} \quad x_* > x_2$$

$$\Delta N = f_N(0, x_*, k_*, x_*, x_1);$$

$$\Delta M = f_M(0, x_*, k_*, x_*, x_1) \quad \text{for} \quad n(x_1) < 0$$

$$\Delta N = f_N(0, x_*, k_*, x_1', x_1);$$

$$\Delta M = f_M(0, x_*, k_*, x_1', x_1) \quad \text{for} \quad n(x_2) < 0. \quad (17b)$$

The hybrid bin method works the same whether the component is water mass, solute mass, or particle shape. Since the particle framework applied in this study has more than one component, the bin shift must be performed in both the water and solute axes for the coalescence process because large drops accrete both water and solute mass from small drops. All of the components are independent of each other, so we applied a "directional splitting" method that amounts to the separate evaluation of the bin shift along each component axis.

The hybrid bin method can also be applied to the spatial distribution of particles. One special implementation of the spatial components is the gravitational "advection" (sedimentation) of particles. If the particle distribution within a spatial grid were not taken into account, precipitation would tend to propagate downward too fast due to numerical diffusion. The spatial bin component is taken exactly the same as the vertical spatial coordinate. Each group of particles has a height variable that has a value within the range of its spatial bin limits.

3. Microphysics

a. Liquid-phase microphysics

The liquid-phase microphysical processes included in the model are the deliquescence and activation of soluble aerosol particles and the growth of drops by condensation and collision–coalescence. Since the basic theory of these processes has been well explained already (e.g., Pruppacher and Klett 1978), only the special schemes applied in this study are described here.

1) CONDENSATIONAL GROWTH

The growth of cloud condensation nuclei (CCN) into cloud drops is calculated explicitly in this study from an initial CCN spectrum that may be either a prescribed function or obtained from observations. We first consider the deliquescence of dry particles into their wet (haze) state, as well as the hysteresis cycle (Chen 1992, 18–24). Since large haze particles have large condensation time constants (Chen 1992, p. 164), one cannot assume that all haze particles reach their equilibrium sizes on the Köhler curves within a typical time step. Kinetic calculations are thus applied to the condensational growth of both the haze particles and cloud drops. The activation of haze particles into cloud drops, then, is automatically accounted for by properly solving the growth equations.

A difficulty commonly encountered in the simulation of condensation and evaporation processes using a bin (category) model is the large number of equations needing to be solved simultaneously. The total number of equations for a sizable particle framework can be too large for differential equation solvers based on matrix methods. It is thus necessary to use special numerical methods for the diffusional growth problem. Clark (1973) applied a semianalytical method to calculate a time-averaged saturation ratio during one time step. This method avoids some numerical instability problems and allows the use of relatively large time steps. In this study, we applied a similar approach by using *Brown's quadratic exponential smoothing* method (Brown 1963, pp. 140–144), a technique that makes forecasts based on past values, to give more efficient and accurate predictions of the supersaturation (Chen 1994). A special method is then used to solve the diffusional growth equation (see appendix). The temperature of the droplets is calculated by assuming steady-state heat and mass transfer (cf. Pruppacher and Klett 1978, p. 420).

2) HYDRODYNAMIC INTERACTIONS

The growth of cloud droplets by collision–coalescence is calculated using the stochastic approach of Telford (1955) to solve the collection equation, given earlier as (4) (cf. Berry 1967; Tzivion et al. 1987). The numerical results of de Almeida (1979) are used for the collision efficiencies, while the empirical relationship of Low and List (1982a) is used for the coalescence efficiencies. The empirical formulas of Low and List (1982b) and List et al. (1987) are used for the distribution function of liquid fragments following drop breakup. Adjustment on the mode of their distribution functions was made to ensure mass conservation (Chen 1992, p. 38). For the redistribution of solute in the drop fragments, it is assumed that when one of the parent drops gains mass during a collision event, it does not contribute any of its original mass to the fragment drops. In this case, the mass of the fragment drops must be from the other parent drop, the one that also provided the extra mass to the first parent drop. If both of the parent drops lose mass, neither one gains any mass or solute from the other, and their original concentrations are preserved. The fragment drops are then assumed to have the same concentration of the mixture of the masses that were stripped away from the parent drops.

A drop may also break up spontaneously without interacting with other drops. An upper limit of 4.5 mm (spherical equivalent radius) is set as the largest stable drop size, a threshold established by the wind tunnel measurements of Pruppacher and Pitter (1971). Any

drop that exceeds this size, because it either grew by coalescence or arose from the melting of ice or shedding during riming, is assumed to break up spontaneously. The breakup size distribution follows the formula given by Srivastava (1971), and all fragment drops retain the solute concentration of the parent drop.

b. Ice-phase microphysics

In this study, we included the ice-phase processes of primary ice nucleation, diffusional growth, hydrodynamic collection (riming), melting, drop shedding during wet growth, aggregation, and secondary generation of ice particles. Special attention has been paid to the determination of the shapes of the ice particles for each growth process.

1) ICE NUCLEATION

Four types of common ice nucleation processes are considered in this study—heterogeneous deposition (or sublimation) nucleation, homogeneous freezing, heterogeneous freezing, and contact nucleation. Homogeneous deposition nucleation is not likely in the atmosphere and is not considered here. Except for the homogeneous freezing, all three other nucleation processes require the presence of ice nuclei (IN). Yet the properties and distribution of IN in the atmosphere are not well known. Georgii and Kleinjung (1967) suggested that large aerosol particles (LAP), with radii greater than 0.1 μm, are potential ice nuclei (IN), and that the IN to LAP ratio is about 1/400 at -20°C. Fletcher (1962) gave the effective IN concentration approximation as

$$N_{\text{IN}} = A \exp(b\Delta T), \tag{18}$$

where A and b are constants, and $\Delta T = T - T_0$ is the deviation of the temperature T from $T_0 = 0$°C. The typical concentration of effective IN in the atmosphere is one per liter at -20°C, and saturation with respect to liquid water is generally assumed. Combining Fletcher's formula and the IN to LAP ratio, we can estimate the number concentration of LAP (*potential* IN) to be about 400 per liter. Young (1974b) deduced the number concentration of contact nuclei to be 230 per liter from Blanchard's (1957) experimental data, which is of the same order of magnitude as the estimated LAP number concentration. Therefore, the LAP are assumed to serve as contact nuclei as well in this study, with a number concentration of 400 per liter that is independent of temperature.

As indicated in (18), Fletcher suggested that the effectiveness of LAP to act as IN is a well-defined function of temperature. Gagin (1972) and Huffman (1973) found, in contrast to Fletcher's suggestion, that the number concentration of effective IN increases with the supersaturation over ice s_i, according to the relationship

$$N_{\text{IN}} = Cs_i^k, \tag{19}$$

where C and k are constants. The temperature dependence in Fletcher's finding is merely a reflection of the temperature dependence of ice supersaturation when liquid water saturation is maintained (Huffman 1973). We have thus adopted the more general supersaturation approach (19), which is converted into a rate equation in terms of the time rate of change of supersaturation

$$\frac{dN_{\text{IN}}}{dt} = N_{\text{IN}}k \frac{d \ln s_i}{dt}. \tag{20}$$

The effective IN considered in (20) are assumed to nucleate immediately and to be removed from the LAP population. Also, it is assumed that the nucleation process is irreversible (i.e., a decrease in supersaturation does not result in a decrease in the number concentration of ice particles) and that $dN_{\text{IN}} \geq 0$.

The other modes of ice nucleation were treated as follows. The scheme of Slinn and Hales (1971) is used to calculate the rate of contact nucleation through thermophoretic and diffusiophoretic transport and Brownian diffusion, using LAP as contact nuclei. For the homogeneous freezing of droplets, an empirical fit to the data presented in Fig. 9 of DeMott and Rogers (1990) is used for the nucleation rate (in cm^{-3} s^{-1}):

$$J_{\text{hom}} = 8 \times 10^4 \exp[-1.75(\Delta T + 34)]. \tag{21}$$

The rate of heterogeneous (immersion) freezing (in cm^{-3} s^{-1}) is calculated using the empirical formula of Danielsen et al. (1972), which is expressed in terms of the cooling rate:

$$J_{\text{het}} = -\gamma \exp[-\gamma(\Delta T + 7)] \frac{dT}{dt} \quad \Delta T \leq -7\text{°C}, \tag{22}$$

where $\gamma = 0.68$ K^{-1}, and $J_{\text{het}} = 0$ when $\Delta T > -7$°C. Again, it is assumed that the nucleation process is irreversible and that $J_{\text{het}} \geq 0$.

2) DIFFUSIONAL GROWTH

The growth of ice crystals by vapor deposition is more complicated than that of droplets, partly because of their nonspherical shapes. The nonspherical shape of an ice crystal introduces complicated boundary conditions, which impose great difficulty in solving the Laplace form of the diffusion equation (Chen and Lamb 1994). However, Jayaweera and Cottis (1969) have shown that spheroids are good analogs for simple columnar and platelike ice crystals. Therefore, the shapes of all types of ice particles are approximated by spheroids in this study.

By examining the crystal surface kinetic and gas phase diffusion effects, Chen and Lamb (1994) theoretically derived the governing equation for the shape change of ice crystals due to depositional growth and showed to first approximation that the differential growths along the c and a axes can be written as

$$\frac{dc}{da} = \Gamma\phi, \tag{23}$$

where Γ is the inherent growth ratio and $\phi = c/a$ is the aspect ratio. The inherent growth ratio Γ is the ratio of the condensation coefficients for the basal and prism faces and is primarily a function of temperature. The effect of ventilation on the shape changes is also included in the scheme. The above equation, when expressed in an integrated form ($c \propto a^{\Gamma}$), has great resemblance to the empirical power-law formulas derived from observational data (e.g., Ono 1970). Moreover, the observed values for the exponent in the integrated relationship match very well with the inherent growth ratio measured in the laboratory. By combining (23) with the mass growth equation, Chen and Lamb also provided a realistic way to describe the change of mass, volume, and shape of ice crystals simultaneously in response to different environmental conditions. They also showed that the change of ϕ due to vapor deposition is loglinear. Thus, the simple pregrowth linear method [section 2b] can be used for the bin shift of particle shape when log ϕ is used as the component axis. All such aspects of the depositional growth process are included in the current model.

3) Growth by collection

The stochastic approach is again used to treat the hydrodynamic interactions between an ice crystal and other particles. The collision efficiencies for ice crystals of different habits collecting small drops (Pitter and Pruppacher 1974; Schlamp et al. 1975; Pitter 1977), as well as the collision efficiencies for large raindrops collecting ice crystals (Lew and Pruppacher 1983; Lew et al. 1985), are compiled into a lookup table as functions of the particle Reynolds number. The coalescence efficiency for droplets in contact with ice particles is assumed to be unity. The density of the rime ice follows the empirical formula of Heymsfield and Pflaum (1985), with impact velocities from Rasmussen and Heymsfield (1985). The shapes of rimed ice particles are simplified in such a way that all droplets are accreted along the short axis (i.e., fixed long-axis length). It can be shown that, with a fixed long-axis length, the shape change due to riming is linear in log(ϕ) scale such that the pregrowth linear method can be used for the bin-shift scheme.

The lookup table mentioned above is also used for the collision efficiencies between two ice crystals, except that the Reynolds number of the collected crystal is used in place of that of the collected drop. The efficiency of crystals to aggregate after collision is not well known, but Mitchell (1988, Table 1) has shown that the aggregation efficiency E_{agg} is dependent on the habits and physical structure of the crystals. The more intricate the shape, the greater the magnitude of E_{agg} becomes. We found that the relationship

$$E_{agg} = 1 - \rho_i/\rho_0 \tag{24}$$

fits Mitchell's data fairly well. Here, ρ_i is the apparent crystal density given by Chen and Lamb (1994), and ρ_0 is the bulk density of ice. Since aggregation involves two ice crystals with different apparent densities, the volume-weighted mean density of the two crystals is used for ρ_i in (24).

The change of ice particle shape due to aggregation is also poorly known. Mitchell et al. (1990) showed a mass-dimension relationship for snow aggregates in the form of $m = \alpha D^{\beta}$, which can be expressed in a differential form:

$$\frac{dD}{D} = \frac{1}{\beta}\frac{dm}{m}. \tag{25}$$

where m is the crystal mass, D is the crystal maximum dimension (major-axis length), and α and β are coefficients that vary with crystal type. The values of β ranged from 1.7 to 2.5, with a mean around 2. The mass-dimension relationship (25) applies to snow aggregates consisting of many single crystals. At the other extreme, for crystal aggregates consisting of only two single crystals, Higuchi (1960), Kajikawa (1985), and Kajikawa and Heymsfield (1989) showed that the "separation ratio,"

$$S = \frac{2L}{D_1 + D_2}, \tag{26}$$

representing a normalized distance between two platelike crystals that are in plane contact, has its highest frequency between about 0.55 and 0.65, where L is the distance between the centers of the two combined crystals having maximum dimensions D_1 and D_2. For crystals of similar size and mass (i.e., $D_1 \approx D_2 = D$, $m_1 \approx m_2 = m$), the increase in particle dimension dD that results from the collection of the second crystal is simply L, so (26) allows us to state

$$\frac{dD}{D} \sim S. \tag{27}$$

Comparison of (27) with (25) suggests, for crystals of similar mass ($dm = m$), that the magnitudes of S and $1/\beta$ should be comparable. The available data, however, show that $1/\beta$ is typically somewhat less than S. Strictly, (26) applies to crystal pairs that are in plane contact. Ice crystals with more complicated structures may combine at a certain intersection angle θ. The magnitude of θ should vary with the shapes of the colliding crystals, and it could be quite large for crystals that are highly branched and of low apparent densities. When a certain crossing angle exist, S of the crystal pairs would become closer to $1/\beta$.

Equations (25) and (27) do not account for the changes in the minimum dimensions (minor-axis length) of the crystal aggregates, but such information is also required for determining the aspect ratio of the

crystal aggregate for this study. By considering (25) and (27) and the geometry of crystals crossing at an arbitrary angle θ, we find that the changes in the long (major) and short (minor) axis lengths due to the collection of a crystal with long and short axis lengths of D_L and D_S, respectively, can be parameterized as

$$\delta D_L \approx [\lambda D_S + \lambda' D_L]\cdot S$$
$$\delta D_S \approx [\lambda D_L + \lambda' D_S], \quad (28)$$

where $\lambda = \sin\theta$, $\lambda' = \cos\theta = \sqrt{1-\lambda^2}$, and S is set equal to 0.6. As a first-order approximation, λ is assumed to be linearly dependent on the volume-weighted crystal apparent density (smaller θ for a higher ρ_i), such that

$$\lambda = \lambda_{\max}(1 - \rho_i/\rho_0), \quad (29)$$

where $\lambda_{\max}$ corresponds to the crossing angle having a maximum probability. We assume this most likely angle to be about 45°, so we set $\lambda_{\max} = 0.7$. The parameterization scheme (28) guarantees a lower apparent density and a more spherical shape for crystals that grow by aggregation.

4) MELTING AND SHEDDING

In this study, we keep track of the total heat (enthalpy) of the ice particles, as modified by vapor deposition, riming, melting, and heat conduction to/from the air. As for droplets, the assumption of steady-state heat and mass transfer is applied (Chen 1992, 177–179). The total heat is defined as the sum of the latent heat and sensible heat (integrated from a reference state at $T_0 = 0$°C). We decide whether meltwater exists in an ice particle according to the criterion

$$h_i(T) > h_i(T_0) \equiv 0, \quad (30)$$

where h_i is the specific total heat of the ice particle and $h_i(T_0)$ is the specific total heat of ice at 0°C. Such a criterion simply means that if the total heat of the particle exceeds that of a bulk ice particle with the same mass at 0°C, the excess heat must be from the unfrozen part of the particle. The mass of the meltwater is then determined by reexamining the total heat of the particle:

$$H_i = m_w h_w(T_0) + m_i h_i(T_0), \quad (31)$$

where $h_w(T_0)$ is the specific total heat of water at 0°C and m_w and m_i are the liquid and solid portions of the mass, respectively. Since we use the thermodynamic melting point (T_0) as the reference state, $h_i(T_0) = 0$, and since $h_w(T_0) = h_i(T_0) + l_f(T_0) = l_f(T_0)$, we have

$$m_w = \frac{H_i}{l_f(T_0)}, \quad (32)$$

where l_f is the latent heat of freezing. The liquid water tends to fill in the available void spaces in the ice particle under conditions of *spongy growth*. Note that, with the depositional density and the rime density given, this model also considers the apparent (circumscribed) volume of ice particles and, thus, the void spaces.

When no more porous space is accessible, meltwater will accumulate on the surface of the ice particle and form a layer of water over the ice surfaces when the diameter of the ice core is less than 9 mm (Rasmussen et al. 1984). The aspect ratio of such ice particles is assumed to be the same as the ice core. Those with larger cores, however, tend to form a water torus near the equator of the particles (Rasmussen et al. 1984). In this case, the short-axis length is kept constant while the meltwater accumulates along the long axis. *Shedding* may occur when the mass of the water torus is greater than the critical mass (Rasmussen and Heymsfield 1987):

$$m_w^* = 0.268 \pm 0.1389 m_{\text{core}}, \quad (33)$$

where m_{core} is the mass (in g) of the ice core including the unfrozen part. An empirical fit to Fig. 8 of Rasmussen et al. (1984) is used to determine the amount of water shed:

$$m_{\text{shed}} \approx m_w - m_t/[1 + 10.67(d - 0.9) - 10.81(d - 0.9)^2 + 10.26(d - 0.9)^3], \quad (34)$$

where m_t is the total mass of the particle and d is the diameter of the ice core in centimeters. The water that is shed is then turned into raindrops. The number and size distribution of the shedded drops are not well studied, so we adopt the spontaneous breakup scheme for liquid drops in determining their size distribution.

The shedding of drops during melting is treated similar to the rime–shedding process. The melting of the ice particles is assumed to occur preferentially along the long axis of the ice core. Such an arrangement is also meant to simulate the melting of dendrites or needles from their tips first. The freezing of wet ice is taken to be exactly the opposite of the melting process.

The depression of the melting point due to the presence of solute (cf. Atkins 1986, 172–173) is also considered in this study. This process is important for evaporating ice particles. The loss of water mass during evaporation leads to an increase of solute concentration and eventually to a state such that the remainder of the ice particle melts at subfreezing temperatures and exists as a haze particle. The presence of solute may also suppress the homogeneous freezing process, especially for haze and interstitial aerosol particles (Sassen and Dodd 1988, 1989; Heymsfield and Miloshevich 1993).

5) SECONDARY ICE PRODUCTION

Of the three types of fragmentation processes that can occur during ice-phase hydrodynamic interactions and melting, the one that creates new liquid-phase par-

ticles (shedding) has already been discussed. The other two processes produce new, "secondary" ice particles via *rime–splintering* (Mossop et al. 1972; Hallett and Mossop 1974) and *collision–fragmentation* (Hobbs and Farber 1972; Vardiman 1978). For the rime–splintering process, we adopted the scheme of Gordon and Marwitz (1981) and Cotton et al. (1986), who used the data from Mossop (1976) to give the number of splinters produced for every 250 drops with diameter > 24 μm as a function of temperature. Fragmentation is not included in this study.

4. Chemistry

a. Liquid-phase chemistry

The characteristic times for ionic dissociation are much smaller than for any other chemical or microphysical process considered in this study. Thus, ionic dissociation is considered to reach equilibrium instantaneously within a typical time step. We therefore reduce the number of equations by combining related ions into a single species. For the reactions considered in this study, $CO_2 \cdot H_2O$, HCO_3^-, and CO_3^{2-} are grouped as the C(IV) species; $NH_3 \cdot H_2O$, and NH_4^+ are the N(III) species; $SO_2 \cdot H_2O$, HSO_3^-, and SO_3^{2-} are the S(IV) species; and HSO_4^- and SO_4^{2-} are the S(VI) species. The aqueous-phase oxidation of S(IV) by H_2O_2 and O_3 is also considered. The dissociation coefficients and rate constants used here are from Pandis and Seinfeld (1989).

Many cloud chemistry models have assumed that an equilibrium is maintained between the gas and aqueous phase at all times (e.g., Möller and Mauersberger 1992). However, Walcek and Pruppacher (1984), Hill (1988), Rood and Currie (1989), Shimshock (1989), and Wexler and Seinfeld (1990) showed that Henry's law equilibrium does not always exist between water drops and the air. In this study, we use a more detailed mass transfer approach for the liquid-phase chemistry, one that does not assume gas–liquid equilibrium (e.g., Schwartz 1986; Jacob 1986; Pandis and Seinfeld 1989).

The differential equations describing the mass transfer and chemical reactions are usually stiff in nature. Moreover, for category models, each drop category requires a separate set of these equations. Thus, special numerical techniques are normally required. Here, we adopted the predictor–corrector method of Young and Boris (1977) to solve the equations of mass transfer and chemical reactions simultaneously.

The shift of the drop spectrum in the solute component, either due to sorption or internal chemical reactions, is similar to its shift in the water component due to condensation. However, the mass change of the major solute (component variable) due to chemical processes depends on the solute concentration and the drop size, not on the absolute solute mass. A bin shift (section 2b) in the solute component inevitably involves the properties in the water component and creates the problem of "component crossing." Nevertheless, the production of sulfate due to sorption or aqueous-phase reactions is normally small compared with the existing sulfate in the drop for a typical time step. So, to a first approximation, we assume that the rate of change of solute mass is fixed for all drops in the same bin so that the shift of the bin limits is the same as the shift of the mean. Note, however, that the postgrowth linear, instead of the pregrowth linear, method would nevertheless have to be used for the bin shift scheme if the solute axis were to be gridded nonlinearly (e.g., log spacing). On the other hand, the shift of the particle spectrum in the solute component due to processes that involve other particles (e.g., coalescence, riming) depends on the amount of solute contained in the collected particles. In this case, the process is the same as that for the shift in the water component, with solute mass replacing water mass in the growth equations. The same principle applies to the ice-phase processes.

b. Ice-phase chemistry

The chemistry that occurs in the ice phase is often thought to be less important than that in the liquid phase, so it is ignored in most cloud chemistry models. Yet, there is increasing evidence that the ice-phase chemistry cannot be totally neglected (e.g., Borys et al. 1988; Chen and Lamb 1990). Also, trace chemicals may affect the growth or evaporation of ice crystal (Chen and Crutzen 1994). Therefore, for a cloud chemistry model to be complete, it must include the ice-phase chemistry. In this study, we have focused on the physical processes that control the removal of trace chemicals by ice-phase precipitation. The chemical reactions occurring in the ice phase or on the particle surfaces are potentially important, but they are not included at this stage due to their complicated nature and a general lack of information.

The diffusion process not only occurs between the gas and liquid phases but also between the gas and ice phases in clouds. Although solute tends to be excluded from the bulk ice (Gross 1968) and remain on the surface of ice particles, the large surface to volume ratios of the ice particles makes them potentially good candidates for removing trace chemicals from the air. Several experimental studies have been conducted to explore the sorption of SO_2 into ice (e.g., Sommerfeld and Lamb 1986; Clapsaddle and Lamb 1989; Valdez et al. 1989). Chen and Lamb (1990) compiled these results into empirical formulas, among which we have adopted the following expression:

$$[\mathrm{S(IV)}]_{\mathrm{dep}} = c \exp\left(\frac{d}{T}\right) P_{\mathrm{SO_2}}^{1/2}, \qquad (35)$$

where $[\mathrm{S(IV)}]_{\mathrm{dep}}$ is the S(IV) concentration in the va-

por-grown ice, P_{SO_2} is the partial pressure of gaseous SO_2, $c = 8.0 \times 10^{-8}$ M atm$^{-1/2}$, and $d = -6.06 \times 10^3$ K. This formula interprets sorption as a bulk process instead of a surface phenomenon. The sorption concentrations for other trace chemicals, as well as the interactions between them, are not well known and need further experimental investigation before they can be included in the model.

Riming causes ice particles to collect not only water but also some of the solutes contained in the cloud drops. The fast propagation of ice within the supercooled drops during the adiabatic stage of freezing may result in the physical entrapment of the dissolved gases. Past studies of gaseous entrapment in freezing water drops have been sparse. Lamb and Blumenstein (1987), as well as Iribarne and Pyshnov (1990), measured the fraction of S(IV) solute retained during freezing. Here, we have adopted the expression of Lamb and Blumenstein for this entrapped fraction, the *retention coefficient:*

$$f_{S(IV)} = 0.012 + 0.0058\Delta T, \qquad (36)$$

where $\Delta T = T_0 - T_w$ is the drop supercooling and T_w is the drop temperature just prior to impact. Iribarne et al. (1990) measured the retention of HCl, HNO_3, NH_3, and H_2O_2, and found that these chemicals were totally retained in the ice after freezing. However, Snider et al. (1992) suggested that the freezing rates given by Iribarne et al. (1990) were too high and that some H_2O_2 is released to the gas phase during riming in natural clouds. Here, we have adopted the retention coefficients for H_2O_2 ($f_{H_2O_2} = 0.24$) given by Snider et al. (1992).

5. Preliminary tests

The *hybrid bin method* has been tested on some idealized cases, and the results have been compared with existing analytical solutions to check the computational integrity and efficiency of the method. The first test considered the evolution of a drop spectrum due to evaporation, using the following simplified growth kernel (11). The analytical solution for the drop number distribution as a function of time, mass, and the original number density function at $t = 0$ has been given by Tzivion et al. (1989). The function, from Berry (1967),

$$F(X, t = 0) = 4X \exp(-2X), \qquad (37)$$

is used as an initial drop spectrum, where $X = m/m_0$ is the mass normalized to the mode of the distribution m_0 ($=2.8 \times 10^{-4}$ g, equivalent to a radius of 400 μm). The accuracy of the simulated results, as shown in Fig. 5, is similar to that of Tzivion et al. (1989), who did a similar comparison using the method of moments. The hybrid bin method is fairly accurate for the condensation/evaporation equation even with a time step as large as 100 s. The accuracy does not improve much with smaller time steps.

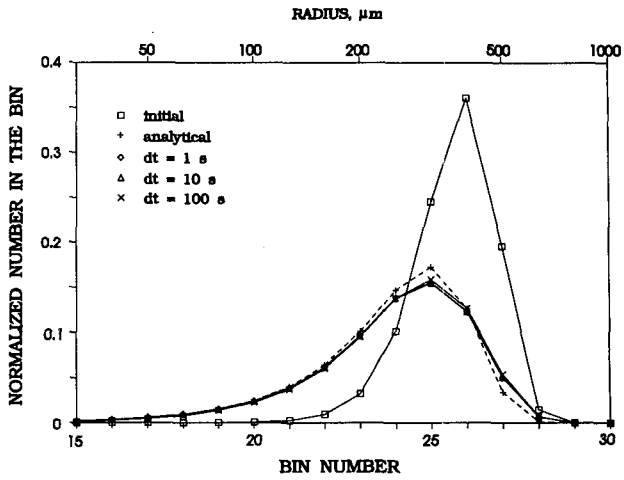

FIG. 5. Comparisons of the results from the hybrid bin method with an analytical solution for the evolution of drop number distribution due to evaporation. The air humidity is fixed at 70%. The result shown is after 50 min of simulation time. The top axis is the drop radius, the bottom axis is the bin number, and the vertical axis is the number of particles in each bin normalized to the total number.

The hybrid bin method was also tested for the growth of droplets by coalescence. The time-dependent stochastic coalescence equation can be idealized by selecting a constant collection kernel K_0 so that analytical solutions are available. The drop distribution function used is the same as that in the previous test but with a mode $m_0 = 4.18 \times 10^{-9}$ g (equivalent to 10 μm in radius) to represent a cloud drop population. Analytical solution of the time-dependent drop spectrum for a constant kernel and the initial drop spectrum (37) can be found in Bleck (1970). Figure 6 shows the results for a constant kernel of $K_0 = 1.8 \times 10^{-4}$ cm^3 s^{-1}. The results from the hybrid bin method, with a bin-sizing factor of 2, very closely follow the analytical solutions, and the accuracy is similar to that of Tzivion et al. (1987). The results are similar for time steps of 1, 3, and 10 s.

Another test was performed with the nonlinear Golovin's kernel $K(x, y) = b(x + y)$, where b is a constant. This kernel is somewhat more realistic than the constant kernel because of the drop mass dependence. Berry (1967) provided an asymptotic approximation for the solution for the drop spectrum evolving from the initial exponential distribution function:

$$g(\ln r) = 3N_0 m_0 X^2 \exp(-X). \qquad (38)$$

Figure 7 demonstrates the evolution of the drop spectrum after 30 and 50 minutes for $b = 1530$ cm^3 g^{-1} s^{-1} using a bin-sizing factor of $\sqrt{2}$. A fairly good agreement with the quasi-analytical solution is also achieved. When using a bin-sizing factor of 2, however, the evo-

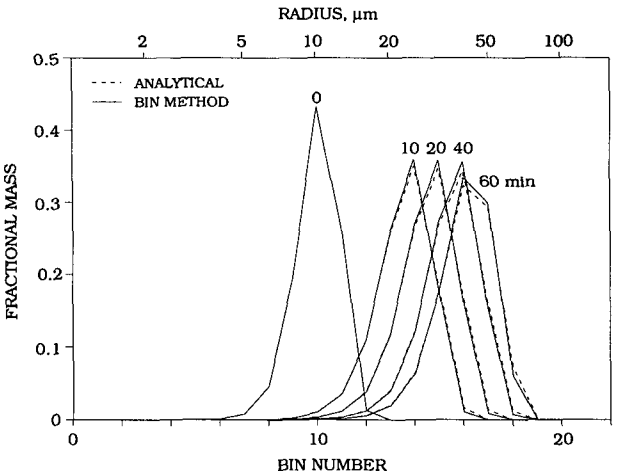

FIG. 6. Comparison of the stochastic collection computations for a constant kernel of $K_0 = 1.8 \times 10^{-4}$ cm^3 s^{-1}. The spectra are for simulation times of 0, 10, 20, 40, and 60 min. The bottom axis is the bin number. The vertical axis is the fractional mass in each bin. The analytical solutions are represented by the dashed lines and the hybrid bin method by the solid lines.

lution of the spectrum is about two bins slower at 50 min than the actual solution. Such error is mainly due to the nonlinear nature of the interaction between particles that each have a different distribution function. Correction can be made by applying a more complicated scheme (Chen 1992, 144–148), which is by nature close to the method of moments of Tzivion et al. (1987) and is more time consuming. We elect to use the less complicated *hybrid method* with higher bin resolution for several reasons. First, the form of the actual collection kernel is much more complicated than the Golovin kernel. The stochastic collection equation is virtually impossible to be solved with complicated schemes such as the method of moments. Furthermore, our current understanding of the realistic collection kernel is still quite poor. It does not pay to use a complicated numerical scheme when the equation to be solved has great uncertainties. Although using a higher bin resolution seems to introduce more interaction between bins, the straightforward hybrid method actually takes less time for each interaction and tends to compensate for the overall increase in the number of calculations. Moreover, this hybrid scheme is very flexible so that a varying bin-sizing factor can be easily applied. Since the coalescence process is important only for drops with relatively large sizes, the bin-sizing factor can be arranged in a way that higher resolution is given to the larger end of the size spectrum and less to the smaller end. Thus, the total bin number was reduced to a manageable magnitude (45 in this study) without sacrificing much accuracy for the coalescence process.

An extended test of the hybrid bin method was performed by applying realistic collision and coalescence kernels and the breakup scheme mentioned in section 3. This test is designed to focus on the details of the raindrop size distribution. A conventional parameterization for the raindrop size spectrum used in bulk water cloud models assumes the empirically obtained Marshall–Palmer distribution (Marshall and Palmer 1948):

$$n(d) = N_0 \exp(-\Lambda d), \qquad (39)$$

where d denotes drop diameter (mm), $N_0 = 8 \times 10^{-6}$ mm^{-4}, and Λ is the slope of the loglinear distribution function, which can be determined from the rate of rainfall. This exponential function is accurate only to a first order. Using the detailed spectral (bin) method and the realistic coalescence and breakup schemes, we are able to uncover the finer details of the raindrop size distribution. This test was performed by letting an initially Marshall–Palmer distribution evolve with time. As shown in Fig. 8, the evolution of the drop spectrum starts with the breakup of large drops and the creation of submillimeter-size small drops. While the number of large drops decreases continuously, the number of small drops oscillates toward an equilibrium value. The whole spectrum becomes quite stable after about 30 min and evolves into a trimodal distribution. This result is in good agreement with the numerical simulations of Valdez and Young (1985), List et al. (1987), and Brown (1988, 1989).

Other tests of the hybrid bin method applied in a multicomponent framework have been done in previous studies, as summarized here. The hybrid bin method was used to study the effect of cloud microphysics on the composition of rain with a liquid-phase particle framework that has two components—water mass and solute mass (Chen and Lamb 1992). The evolution of the two-dimensional drop spectra due to various microphysical processes was demonstrated. It was also shown that drops of the same size do not necessarily have the same amount of solute and vice versa.

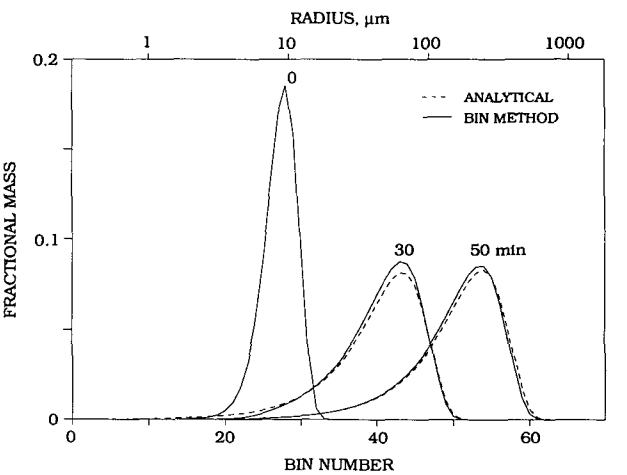

FIG. 7. Same as Fig. 6 but for Golovin's kernel.

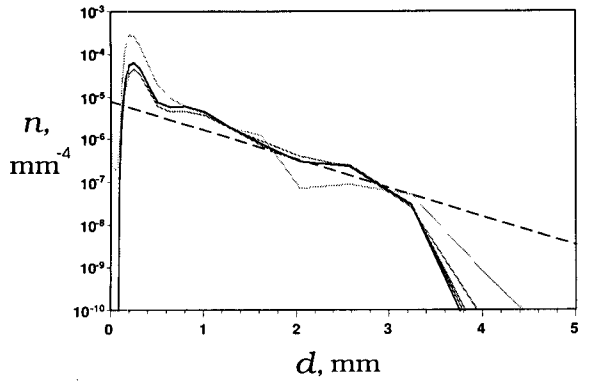

FIG. 8. Trimodal drop size spectrum evolved from an initial Marshall–Palmer-type distribution (dashed line) with realistic coalescence kernel and breakup scheme. The shade of the curves indicates the time of simulation, with 10-min increment for each level of line density. The darkest line shows the drop size spectrum at 50 min of simulation time.

Such multicomponent nature of the compositions of cloud drops and rain may be important to the chemical processes in clouds. For the ice-phase microphysics, Chen and Lamb (1994) applied an ice particle framework with water mass and crystal aspect ratio as its two components. With an adaptive parameterization scheme, they were able to simulate the evolution of the two-dimensional (mass and aspect ratio) spectrum of ice crystals under varying ambient conditions, as well as the shift of crystal habits under different temperature regimes.

6. Summary

A multicomponent, multiphase model has been developed to study the effects of cloud microphysical processes on the redistribution of atmospheric trace substances. This multicomponent particle framework categorizes the distribution of liquid-phase particles according to their water and solute masses. An additional shape factor (aspect ratio) was applied to the categorization of ice-phase particles. A hybrid bin method, which is similar to the method-of-moments scheme, was applied in the multicomponent particle framework to ensure fast and accurate calculation of the particle growth.

The physical and chemical processes have been treated explicitly in this study. The processes for the growth of liquid-phase particles include deliquescence of dry particles into haze drops, which then can grow by condensation into cloud drops. Cloud drops may coalesce while colliding with each other and form larger, precipitable drops (raindrops). Raindrops may continue to collect smaller drops or break up during collision. A set of basic liquid-phase chemical processes was included without relying on the assumption of Henry's law equilibrium between the gas and liquid phases.

Special efforts have been put on the growth and habits of the ice crystals. A theoretically derived parameterization scheme, which is in good agreement with observational data, was applied to describe the time evolution of the habits of ice crystals grown by vapor deposition. Ice crystals are also allowed to grow by accreting cloud droplets (riming). Shedding may occur during heavy riming or melting, when liquid water starts to accumulate on the surface of ice particles. The shape changes of ice particles during riming, shedding, melting, and aggregation have also been considered. This model has been developed with emphasis on the physical and chemical mechanisms and their interactions in clouds. As such, the model proves to be a useful tool for testing the relative importance of processes studied in the laboratory. Some recent laboratory results on the ice-phase chemical processes (trace gas sorption and entrapment in rime ice) have been parameterized and included in the model.

Because of the amount of detail included, this model is computationally very intensive. Therefore, a relatively uncomplicated scenario has been chosen for the simulation at this stage. As will be shown in the sequels of this paper, the model is readily adaptable to a number of situations, such as a two-dimensional, steady-state simulation of a wintertime, orographic cloud.

Acknowledgments. This work was supported in various parts by the Department of Energy under Grant DE-FG02-90ER61071 and the National Science Foundation under Grant ATM-8919837. The detailed comments and suggestions of the anonymous reviewers are greatly appreciated. One author (J.-P. Chen) wishes to acknowledge support from the Earth System Science Center, College of Earth and Mineral Sciences, for a fellowship and for the use of its CRAY-YMP computer.

APPENDIX

Numerical Solutions of the Condensation Growth Equation

The condensation growth equation can be written as a first-order, nonlinear differential equation (cf. Clark 1973; Chen 1992, p. 161):

$$\frac{dr}{dt} = \frac{B}{r}\left[s_\infty - \frac{\alpha}{r} + \frac{\beta}{r^3}\right], \qquad \text{(A1)}$$

where s_∞ is the supersaturation and B, α, and β are independent of r. This equation cannot be solved analytically. Numerical techniques, such as the Runge–Kutta method, are usually required (Árnason and Brown 1971; Robinson 1984). Here, a new technique is introduced, one that is accurate and computationally efficient.

For a small enough time step δt, the change of drop radius δr can be approximated by

$$\delta r \approx \overline{\left(\frac{dr}{dt}\right)}\,\delta t. \tag{A2}$$

Here, $\overline{(dr/dt)}$ is the average rate of change of r during δt and can be approximated by applying the *mean value theorem for integrals* (Bak and Lichtenberg 1966, p. 143) such that

$$\overline{\left(\frac{dr}{dt}\right)} = \frac{\int_{r_0}^{r_1} \frac{dr}{dt}\,dr}{\int_{r_0}^{r_1} dr} = \frac{B}{\delta r}\left\{ s_\infty \ln\frac{r_1}{r_0} + \alpha\left(\frac{1}{r_1} - \frac{1}{r_0}\right) - \frac{\beta}{3}\left(\frac{1}{r_1^3} - \frac{1}{r_0^3}\right)\right\} \equiv \frac{B^*}{\delta r}, \tag{A3}$$

where r_0 is the initial drop radius and $r_1 = r_0 + \delta r$ is the radius after δt. We thus have

$$\delta t \approx \frac{(\delta r)^2}{B^*}, \tag{A4}$$

which can be solved iteratively for r_1 using r_0 as the initial guess. However, (A3) is a good approximation only when the change of r is not too large. Since the drop growth rate (A1) varies quite significantly during cloud formation, time step adjustment is normally required for solving either (A1) or (A3). The control of model time step is usually a difficult task for the calculation of drop growth, especially during the activation stage (Árnason and Brown 1971).

A better way to solve (A3) is to calculate δt for a certain increment of r instead. This *time-stepping scheme* limits the change of r during a certain time increment δt such that

$$r_1 = r_0(1 + \xi), \tag{A5}$$

where ξ is a small number and is positive for condensation and negative for evaporation. The growth of the drop can then be calculated by incrementing the drop size according to (A6) with the corresponding integration time step, δt, determined from (A4). The control of δr not only ensures the validity of (A3) but also enables the linearization of the logarithmic term in (A3):

$$\ln\frac{r_1}{r_0} = \ln(1 + \xi) \approx \xi - \frac{\xi^2}{2} + \frac{\xi^3}{3}. \tag{A6}$$

The initial value of $|\xi|$ should normally be 0.05 or less, and needs to be readjusted upon encountering either of two situations. First, there will be times when the overall integration time $\Sigma\,\delta t$ exceeds the model time step Δt, that is, when the current time increment stepped over the remaining integration time step Δt_{rem}. Also, small haze particles may reach their equilibrium size well short of the whole integration time step, and δt (and B^*) might be less than zero as r_1 exceeds the equilibrium size (overgrowth). So, when the condition

$$B^* < \frac{(\delta r)^2}{\Delta t_{\text{rem}}} \tag{A7}$$

is met, a smaller $|\xi|$ should be reapplied for the last integration. The optimal decay factor for ξ is about 0.25 (i.e., $\xi_{\text{new}} = 0.25\xi_{\text{old}}$). The integration process should be repeated until Δt_{rem} or $|\xi|$ is smaller than a certain criterion (e.g., $<10^{-5}$).

For large and diluted drops, the Kelvin and Raoult effects can be ignored, and (A1) can be reduced to

$$\frac{d(r^2)}{dt} = 2r\frac{dr}{dt} \approx 2Bs_\infty, \tag{A8}$$

which has a square-root analytical solution

$$r_1 = \sqrt{r_0^2 + 2Bs_\infty \Delta t}. \tag{A9}$$

Hagen (1979) used the criterion $r > r^{\#} \equiv r^* + 2\ \mu\text{m}$ to decide if the drop can be regarded as large and diluted. The parameter $r^{\#}$ is called the *dividing radius* and r^* is the Köhler curve critical radius.

REFERENCES

Árnason, G., and P. S. Brown Jr., 1971: Growth of cloud droplets by condensation: A problem in computational stability. *J. Atmos. Sci.*, **28,** 72–77.

Atkins, P. W., 1986: *Physical Chemistry.* 3d ed. Oxford University Press, 857 pp.

Ayers, G. P., and T. V. Larson, 1990: Numerical study of droplet size dependent chemistry in oceanic, wintertime stratus cloud at southern mid-latitudes. *J. Atmos. Chem.*, **11,** 143–167.

Bak, T. A., and J. Lichtenberg, 1966: *Mathematics for Scientists.* W. A. Benjamin Inc., 487 pp.

Berry, E. X., 1967: Cloud droplet growth by coalescence. *J. Atmos. Sci.*, **24,** 688–701.

——, and R. L. Reinhardt, 1974: An analysis of cloud drop growth by collection: Part I. double distributions. *J. Atmos. Sci.*, **31,** 1814–1824.

Blanchard, D. C., 1957: The supercooling, freezing and melting of giant waterdrops at terminal velocity in air. *Artificial Stimulation of Rain,* H. Weickmann and W. Smith, Eds., Pergamon Press, 233–249.

Bleck, R., 1970: A fast, approximative method for integrating the stochastic coalescence equation. *J. Geophys. Res.*, **75,** 5165–5171.

Borys, R. D., E. E. Hindman, and P. J. DeMott, 1988: The chemical fractionation of atmospheric aerosol as a result of snow crystal formation and growth. *J. Atmos. Chem.*, **7,** 213–239.

Brown, P. S., Jr., 1988: The effects of filament, sheet, and disk breakup upon the drop spectrum. *J. Atmos. Sci.*, **45,** 712–718.

——, 1989: Coalescence and breakup-induced oscillations in the evolution of the raindrop size distribution. *J. Atmos. Sci.*, **46,** 1186–1192.

Brown, R. G., 1963: *Smoothing, Forecasting and Prediction of Discrete Time Series.* Prentice-Hall, 468 pp.

Charlson, R. J., J. E. Lovelock, M. O. Andreae, and S. G. Warren, 1987: Oceanic phytoplankton, atmospheric sulfur, cloud albedo and climate. *Nature,* **326,** 655–661.

Chen, J.-P., 1992: Numerical simulation of the redistribution of atmospheric trace chemicals through cloud processes. Ph.D. dissertation, The Pennsylvania State University, University Park, PA, 342 pp.

——, 1994: Predictions of saturation ratio for cloud microphysical models. *J. Atmos. Sci.*, **51,** 1332–1338.
——, and D. Lamb, 1990: The role of precipitation microphysics in the selective filtration of air entering the upper troposphere. Preprints, *Conf. on Cloud Physics,* San Francisco, CA, 479–484.
——, and ——, 1992: The effect of cloud microphysics on the composition of rain. *Precipitation Scavenging and Atmosphere–Surface Exchange,* S. E. Schwartz and W. G. N. Slinn, Eds., Hemisphere Publishing, 51–62.
——, and ——, 1994: The theoretical basis for the parameterization of ice crystal habits: Growth by vapor deposition. *J. Atmos. Sci.,* **51,** 1206–1221.
——, and P. J. Crutzen, 1994: Solute effect on the evaporation of ice particles. *J. Geophys. Res.,* in press.
Cho, H. R., M. Niewiadomski, and J. V. Iribarne, 1989: A model of the effect of cumulus clouds on the redistribution and transformation of pollutants. *J. Geophys. Res.,* **94**(D10), 12 895–12 910.
Clapsaddle, C., and D. Lamb, 1989: Laboratory experimentation on the sorption of SO_2-ice system at trace levels. Preprints, *Symp. on the Role of Clouds in Atmospheric Chemistry and Global Climates,* Anaheim, CA, Amer. Meteor. Soc./WMO, 249–252.
Clark, 1973: Numerical modeling of the dynamics and microphysics of warm cumulus convection. *J. Atmos. Sci.,* **30,** 857–878.
——, 1974: A study in cloud phase parameterization using the gamma distribution. *J. Atmos. Sci.,* **31,** 142–155.
Cotton, W. R., G. J. Tripoli, R. M. Rauber, and E. A. Mulvihill, 1986: Numerical simulation of the effects of varying ice crystal nucleation rates and aggregation processes on orographic snowfall. *J. Climate Appl. Meteor.,* **25,** 1658–1680.
Danielsen, E. F., R. Bleck, and D. A. Morris, 1972: Hail growth by stochastic collection in a cumulus model. *J. Atmos. Sci.,* **29,** 135–155.
de Almeida, F. C., 1979: The effect of small-scale turbulent motions on the growth of a cloud droplet spectrum. *J. Atmos. Sci.,* **36,** 1557–1563.
DeMott, P. J., and D. C. Rogers, 1990: Freezing nucleation rates of dilute solution droplets measured between −30°C and −40°C in laboratory simulations of natural clouds. *J. Atmos. Sci.,* **47,** 1056–1064.
Drake, R. L., 1972: The scalar transport equation of coalescence theory: Moments and kernels. *J. Atmos. Sci.,* **29,** 537–547.
Enukashvily, I. M., 1980: A numerical method for integrating the kinetic equation of coalescence and breakup of cloud droplets. *J. Atmos. Sci.,* **37,** 2521–2534.
Fletcher, N. H., 1962: *The Physics of Rainclouds.* Cambridge University Press, 390 pp.
Flossmann, A. I., and H. R. Pruppacher, 1988: A theoretical study of the wet removal of atmospheric pollutants. Part III: The uptake, redistribution, and deposition of $(NH_4)_2SO_4$ particles by a convective cloud using a two-dimensional cloud dynamics model. *J. Atmos. Sci.,* **45,** 1857–1871.
——, W. D. Hall, and H. R. Pruppacher, 1985: A theoretical study of the wet removal of atmospheric pollutants. Part I: The redistribution of aerosol particles captured through nucleation and impaction scavenging by growing cloud drops. *J. Atmos. Sci.,* **42,** 583–606.
Gagin, A., 1972: The effect of supersaturation on the ice crystal production by natural aerosols. *J. Rech. Atmos.,* **6,** 175–185.
Gelbard, F., and J. H. Seinfeld, 1978: Numerical solution of the dynamic equation for particulate systems. *J. Comput. Phys.,* **28,** 357–375.
Georgii, H. W., and E. Kleinjung, 1967: Relations between the chemical composition of atmospherical aerosol particles and the concentration of natural ice nuclei. *J. Rech. Atmos.,* **3,** 145–156.
Giorgi, F., and W. L. Chameides, 1985: The rainout parameterization in a photochemical model. *J. Geophys. Res.,* **90, D5,** 7872–7880.
Golovin, A. M., 1963: The solution of the coagulating equation for cloud droplets in a rising air current. *Bull. Acad. Sci. USSR Geophys. Ser.,* **5,** 482–487.
Gordon, G. L., and J. D. Marwitz, 1981: Secondary ice crystal production in stable orographic clouds over the Sierra Nevada. Preprints, *Eighth Conf. on Inadvertent and Planned Weather Modification,* Reno, NV, 62–63.
Gross, G. W., 1968: Some effects of trace inorganics on the ice/water system. *Trace Inorganics in Water, Adv. Chem. Ser.,* Amer. Chem. Soc., 27–97.
Hagen, D. E., 1979: A numerical cloud model for the support of laboratory experimentation. *J. Appl. Meteor.,* **18,** 1035–1043.
Hall, W. D., 1980: A detailed microphysical model within a two-dimensional dynamic framework: Model description and preliminary results. *J. Atmos. Sci.,* **37,** 2486–2507.
——, and H. R. Pruppacher, 1976: The survival of ice particles falling from cirrus clouds in subsaturated air. *J. Atmos. Sci.,* **33,** 1995–2006.
Hallett, J., and S. C. Mossop, 1974: Production of secondary ice particles during the riming process. *Nature,* **249,** 26–28.
Hegg, D. A., 1989: The relative importance of major aqueous sulfate formation reactions in the atmosphere. *Atmos. Res.,* **22,** 323–333.
——, and P. V. Hobbs, 1988: Some effects of cloud microphysics on cloud chemistry. Preprints, *10th Int. Cloud Physics Conf.,* Bad Homburg, Germany, ICCP/IAMAP, 261–263.
——, and T. V. Larson, 1990: The effects of microphysical parameterization on model prediction of sulfate production in clouds. *Tellus,* **42B,** 272–284.
Heymsfield, A. J., and J. C. Pflaum, 1985: A quantitative assessment of the accuracy of techniques for calculating graupel growth. *J. Atmos. Sci.,* **42,** 2264–2274.
——, and L. M. Miloshevich, 1993: Homogeneous ice nucleation and supercooled liquid water in orographic wave clouds. *J. Atmos. Sci.,* **50,** 2335–2353.
Higuchi, K., 1960: On the coalescence between plane snow crystals. *J. Meteor.,* **17,** 239–243.
Hill, T. A., 1988: Chemical evolution within a cloud model featuring a polydisperse droplet size spectrum. Preprints, *10th Int. Cloud Physics Conf.,* Bad Homburg, Germany, ICCP/IAMAP, 294–296.
Hindman, E. E., II, and D. B. Johnson, 1972: Numerical simulation of ice particle growth in a cloud of supercooled water droplets. *J. Atmos. Sci.,* **29,** 1313–1321.
Hobbs, P. V., and R. J. Farber, 1972: Fragmentation of ice particles in clouds. *J. Rech Atmos.,* **6,** 245–258.
Huffman, P. J., 1973: Supersaturation spectra of AgI and natural ice nuclei. *J. Appl. Meteor.,* **12,** 1080–1082.
Iribarne, J. V., and T. Pyshnov, 1990: The effect of freezing on the composition of supercooled droplets—I. Retention of HCl, HNO_3, NH_3 and H_2O_2. *Atmos. Environ.,* **24A,** 383–387.
——, T. Pyshnov, and B. Naik, 1990: The effect of freezing on the composition of supercooled droplets—II. Retention of S(IV). *Atmos. Environ.,* **24A,** 389–398.
Jacob, D. J., 1986: Chemistry of OH in remote clouds and its role in the production of formic acid and peroxymonosulfate. *J. Geophys. Res.,* **91,** D9, 9807–9826.
Jayaweera, K. O. L. F., and R. E. Cottis, 1969: Fall velocities of plate-like and columnar ice crystals. *Quart. J. Roy. Meteor. Soc.,* **95,** 703–709.
Johnson, D., 1982: The role of giant and ultragiant aerosol particles in warm rain initiation. *J. Atmos. Sci.,* **39,** 448–460.
Kajikawa, M., 1985: Structure and falling motion of early snowflakes. *Ann. Glaciol.,* **6,** 269–271.
——, and A. J. Heymsfield, 1989: Aggregation of ice crystals in cirrus. *J. Atmos. Sci.,* **46,** 3108–3121.
Kessler, E., 1969: On the distribution and continuity of water substance in atmospheric circulations. *Meteor. Monogr., No.35,* Amer. Meteor. Soc., 84 pp.

Lamb, D., and R. Blumenstein, 1987: Measurement of the entrapment of sulfur dioxide by rime ice. *Atmos. Environ.*, **21,** 1765–1772.

——, and J.-P. Chen, 1988: Effects of cloud microphysical processes on trace chemical removal efficiencies. Preprints, *10th Int. Cloud Physics Conf.,* Bad Homburg, Germany, ICCP/IAMAP, 306–308.

——, and ——, 1990: A modeling study of the effects of ice-phase microphysical processes on trace chemical removal efficiencies. *Atmos. Res.,* **25,** 31–51.

Lew, J. K., and H. R. Pruppacher, 1983: A theoretical determination of the capture efficiency of small columnar ice crystals by large cloud drops. *J. Atmos. Sci.,* **40,** 139–153.

——, D. E. Kingsmill, and D. C. Montague, 1985: A theoretical study of the collision efficiency of small planar ice crystals colliding with large supercooled water drops. *J. Atmos. Sci.,* **42,** 857–862.

Lin, Y.-L., R. D. Farley, and H. D. Orville, 1983: Bulk parameterization of the snow field in a cloud model. *J. Climate Appl. Meteor.,* **22,** 1065–1092.

List, R., N. R. Donaldson, and R. E. Stewart, 1987: Temporal evolution of drop spectra to collisional equilibrium in steady and pulsating rain. *J. Atmos. Sci.,* **44,** 362–372.

Low, T. B., and R. List, 1982a: Collision, coalescence and breakup of raindrops. Part I: experimentally established coalescence efficiencies and fragment size distributions in breakup. *J. Atmos. Sci.,* **39,** 1951–1606.

——, and ——, 1982b: Collision, coalescence and breakup of raindrops. Part II: parameterization of fragment size distributions. *J. Atmos. Sci.,* **39,** 1607–1618.

Marshall, J. S., and W. M. Palmer, 1948: The distribution of raindrop spectrometer. *J. Meteor.,* **5,** 165–166.

Miller, T. L., and K. C. Young, 1979: A numerical simulation of ice crystal growth from the vapor phase. *J. Atmos. Sci.,* **36,** 458–469.

Mitchell, D. L., 1988: Evolution of snow-size spectra in cyclonic storms. Part I: Snow growth by vapor deposition and aggregation. *J. Atmos. Sci.,* **45,** 3431–3451.

——, 1991: Evolution of snow-size spectra in cyclonic storms. Part II: Deviation from the exponential form. *J. Atmos. Sci.,* **48,** 1885–1899.

——, R. Zhang, and R. L. Pitter, 1990: Mass-dimension relationships for ice particles and the influence of riming on snowfall rates. *J. Appl. Meteor.,* **29,** 153–163.

Möller, D., and G. Mauersberger, 1992: Cloud chemistry effects on tropospheric photooxidants in polluted atmosphere—Model results. *J. Atmos. Chem.,* **14,** 153–165.

Mossop, S. C., 1976: Production of secondary ice particles during the growth of graupel by riming. *Quart. J. Roy. Meteor. Soc.,* **102,** 45–57.

——, R. E. Cottis, and B. M. Barlett, 1972: Ice crystal concentration in cumulus and stratocumulus clouds. *Quart. J. Roy. Meteor. Soc.,* **98,** 105–123.

Niewiadomski, M., 1989: Sulphur dioxide and sulphate in a three-dimensional field of convective clouds: numerical simulations. *Atmos. Environ.,* **23,** 477–487.

Noone, K. J., R. J. Charlson, D. S. Covert, J. A. Ogren, and J. Heintzenberg, 1988: Cloud droplets: solute concentration is size dependent. *J. Geophys. Res.,* **93**(D8), 9477–9482.

Ogren, J. A., J. Heintzenberg, A. Zuber, K. J. Noone, and R. J. Charlson, 1989: Measurements of the size-dependence of solute concentrations in cloud droplets. *Tellus,* **41B,** 24–31.

Ono, A., 1970: Growth mode of ice crystals in natural clouds. *J. Atmos. Sci.,* **27,** 649–658.

Pandis, S. N., and J. H. Seinfeld, 1989: Sensitivity analysis of a chemical mechanism for aqueous-phase atmospheric chemistry. *J. Geophys. Res.,* **94**(D1), 1105–1126.

Pitter, R. L., 1977: A reexamination of riming on thin ice plates. *J. Atmos. Sci.,* **34,** 684–685.

——, and H. R. Pruppacher, 1974: A numerical investigation of collision efficiencies of simple ice plates colliding with supercooled water drops. *J. Atmos. Sci.,* **31,** 551–559.

Pruppacher, H. R., and R. L. Pitter, 1971: A semi-empirical determination of the shape of cloud and raindrops. *J. Atmos. Sci.,* **28,** 86–94.

——, and J. D. Klett, 1978: *Microphysics of Clouds and Precipitation.* Reidel Publishing Company, 714 pp.

Rasmussen, R. M., V. Levizzani, and H. R. Pruppacher, 1984: A wind tunnel and theoretical study of the melting behavior of atmospheric ice particles. II: A theoretical study for frozen drops of radius < 500 micron. *J. Atmos. Sci.,* **41,** 3, 374–388.

——, and A. J. Heymsfield, 1985: A generalized form for impact velocities used to determine graupel accretional densities. *J. Atmos. Sci.,* **42,** 2275–2279.

——, and ——, 1987: Melting and shedding of graupel and hail. Part I: model physics. *J. Atmos. Sci.,* **44,** 2754–2763.

Robinson, N. F., 1984: The efficient numerical calculation of condensational cloud drop growth. *J. Atmos. Sci.,* **41,** 698–700.

Roelofs, G. J. H., 1992: Drop size dependent sulfate distribution in a growing cloud. *J. Atmos. Chem.,* **14,** 109–118.

Rood, M. J., and R. M. Currie, 1989: Absorption of NH_3 and SO_2 during activation of atmospheric cloud condensation nuclei. *Atmos. Environ.,* **23,** 2847–2854.

Sarma, R. A., 1986: Numerical simulation of the formation and transport of sulfate in convective clouds. Ph.D. dissertation, Colorado State University, Fort Collins, CO, 188 pp.

Sassen, K., and G. C. Dodd, 1988: Homogeneous nucleation rate for highly supercooled cirrus cloud droplets. *J. Atmos. Sci.,* **45,** 1357–1369.

——, and ——, 1989: Haze particle nucleation simulations in cirrus clouds, and applications for numerical and lidar studies. *J. Atmos. Sci.,* **46,** 3005–3014.

Schlamp, R. J., H. R. Pruppacher, and A. E. Hamielec, 1975: A numerical investigation of the efficiency with which simple columnar ice crystals collide with supercooled water drops. *J. Atmos. Sci.,* **32,** 2330–2337.

Schwartz, S. E., 1986: Mass-transport considerations pertinent to aqueous-phase reaction of gases in liquid-water clouds. *Chemistry of Multiphase Atmospheric Systems,* W. Jaeschke, Ed., NATO ASI Series, Springer-Verlag, 415–471.

Shimshock, J. P., 1989: Below-cloud scavenging of ammonia gas and particles at a rural central Pennsylvania site. Ph.D. thesis. The Pennsylvania State University, University Park, PA, 154 pp.

Slinn, W. G. N., and J. M. Hales, 1971: A reevaluation of the role of thermophoresis as a mechanism of in- and below-cloud scavenging. *J. Atmos. Sci.,* **28,** 1465–1471.

Snider, J. R., D. C. Montague, and G. Vali, 1992: Hydrogen peroxide retention in rime ice. *J. Geophys. Res.,* **97**(D7), 7569–7578.

Sommerfeld, R. A., and D. Lamb, 1986: Preliminary measurements of SO_2 absorbed on ice. *Geophys. Res. Lett.,* **13,** 349–351.

Srivastava, R. C., 1971: Size distribution of raindrops generated by their breakup and coalescence. *J. Atmos. Sci.,* **28,** 410–415.

Stieltjes, T. J., 1894: Recherches sur les fractions continues. *Ann. Fac. Sci. Toulouse,* **8,** T1–122.

Telford, J. W., 1955: A new aspect of coalescence theory. *J. Meteor.,* **12,** 436–444.

Topalian, J. H., and D. C. Montague, 1989: A theoretical study of chemical kinetic control in the scavenging of pollutant gases by cloud and rain drops. *J. Atmos. Chem.,* **8,** 1–18.

Tremblay, A., and H. Leighton, 1986: A three-dimensional cloud chemistry model. *J. Climate Appl. Meteor.,* **25,** 652–671.

Tripoli, G. J., and W. R. Cotton, 1982: The Colorado State University three-dimensional cloud/mesoscale model—1982. Part I: General theoretical framework and sensitivity experiments. *J. Rech. Atmos.,* **16,** 85–219.

Tzivion, S., 1980: A numerical solution of the kinetic coalescence equation. Preprints, *Eighth Int. Conf. on Cloud Physics,* Clermont-Ferrand, France, ICCP/IAMAP, 87–90.

——, G. Feingold, and Z. Levin, 1987: An efficient numerical solution to the stochastic collection equation. *J. Atmos. Sci.,* **44,** 3139–3149.

——, ——, and ——, 1989: The evolution of raindrop spectra. Part II: collisional collection/breakup and evaporation in a rainshaft. *J. Atmos. Sci.*, **46,** 3312–3327.

——, G. A. Dawson, and R. C. Bales, 1989: Sulfur dioxide incorporation into ice depositing from the vapor. *J. Geophys. Res.*, **94**(D1), 1095–1103.

Valdez, M. P., and K. C. Young, 1985: Number fluxes in equilibrium raindrop populations: A Markov chain analysis. *J. Atmos. Sci.*, **42,** 1024–1036.

Vardiman, L., 1978: The generation of secondary ice particles in clouds by crystal–crystal collision. *J. Atmos. Sci.*, **35,** 2168–2180.

Walcek, C. J., and H. R. Pruppacher, 1984: On the scavenging of SO_2 by cloud and raindrops: III. A theoretical study of SO_2 washout by rain falling through a pollution plume. *J. Atmos. Chem.*, **1,** 307–324.

Wang, C., and J. S. Chang, 1993: A three-dimensional numerical model of cloud dynamics, microphysics, and chemistry. 1. Concepts and formulation. *J. Geophys. Res.*, **98**(D8), 14 827–14 844.

Wexler, A. S., and J. H. Seinfeld, 1990: The distribution of ammonium salts among a size and composition dispersed aerosol. *Atmos. Environ.*, **24A,** 1231–1246.

Young, K. C., 1974a: A numerical simulation of wintertime, orographic precipitation: Part I. Description of model microphysics and numerical techniques. *J. Atmos. Sci.*, **31,** 1735–1748.

——, 1974b: The role of contact nucleation in ice phase initiation in clouds. *J. Atmos. Sci.*, **31,** 768–776.

Young, T. R., and J. P. Boris, 1977: A numerical technique for solving stiff ordinary differential equations associated with the chemical kinetics of reactive-flow problem. *J. Phys. Chem.*, **81**(25), 2424–2427.